

Disk-Evaporation Fed Corona: Structure and Evaporation Feature with Magnetic Field

Lei Qian

Astronomy Department, Peking University, Beijing, 100871, P.R. China

qianl@vega.bac.pku.edu.cn

B.F. Liu

*National Astronomical Observatories/Yunnan Observatory, Chinese Academy of Sciences,
P.O. Box 110, Kunming 650011, China*

and

Xue-Bing Wu

Astronomy Department, Peking University, Beijing, 100871, P.R. China

ABSTRACT

The disk-corona evaporation model naturally interprets many observational phenomena in black hole X-ray binaries, such as the truncation of an accretion disk and the spectral state transitions. On the other hand, magnetic field is known to play an important role in transporting angular momentum and producing viscosity in accretion flows. In this work, we explicitly take the magnetic field in the accretion disk corona into account and numerically calculate the coronal structure on the basis of our two-temperature evaporation code. We show that the magnetic field influences the coronal structure by its contribution to the pressure, energy and radiative cooling in the corona and by decreasing the vertical heat conduction. We found that the maximal evaporation rate keeps more or less constant (~ 0.03 Eddington rate) while the strength of magnetic fields changes, but that the radius corresponding to the maximal evaporation rate decreases with increasing magnetic field. This predicts that the spectral state transition always occurs at a few percent of Eddington accretion rate, while the inner edge of thin disk can be at $\sim 100R_S$ or even less in the hard state before the transition to the soft state. These results alleviate the problem that previous evaporation models predict too large a truncation radius, and are in better agreement with the observational results of several black hole X-ray binaries, though discrepancies remain.

Subject headings: accretion, accretion disks — black hole physics — magnetic fields — conduction — X-rays: binaries

1. Introduction

X-ray binaries and Active Galactic Nuclei (AGN) are interesting objects in astrophysics and have drawn a lot of attentions since their discoveries. Accretion is widely accepted to be the main energy source of them (Shakura & Sunyaev 1973, hereafter SS73; Pringle 1981; Rees 1984). The thin disk model proposed by SS73 not only successfully solves the energy problems in both X-ray binaries and AGN, but also well reproduces some key features of dwarf novae (Meyer & Meyer-Hofmeister 1984). With the development of observing techniques in recent decades, various types of broad band spectra have been observed in X-ray binaries as well as in AGN. These spectra usually show a two-component feature, that is, a thermal component together with a non-thermal component (see Remillard & McClintock 2006 for a review of X-ray binaries; see Mushotzky, Done & Pounds 1993 for a review of AGN). The thin disk alone, which emits a multi-color blackbody spectrum, is difficult to explain the observed broad band spectra. An additional hot accretion flow is required to produce the high-frequency non-thermal spectrum. Therefore, a two-component model, consisting of an inner advection dominated accretion flow (ADAF, Narayan & Yi, 1994), or radiative inefficient accretion flow (RIAF, Yuan, Narayan & Quataert 2003) and an outer Shakura-Sunyaev disk (SSD, SS73), was proposed to explain the observational spectra and now has been widely adopted in studying black hole binaries (e.g. Esin, McClintock & Narayan 1997; Quataert et al. 1999). However, there are still some debates on what causes the transition between these two kinds of physically different accretion flows and how to determine the transition properties, such as the critical accretion rate, the disk truncation radius, and so on.

These problems have been extensively discussed in many previous studies (Narayan & Yi 1995; Honma 1996; Meyer, Liu, & Meyer-Hofmeister 2000b; Lu et al. 2004). Among these models, only Meyer et al. (2000b) consider the detailed vertical structure (a thin disk sandwiched by the corona) concerning the transition between a SSD and a RIAF. It also predicts a scale free evaporation rate-radius ($\dot{m} - r$) relation, with which the disk truncation radius is determined for a given accretion rate and is found to be consistent with observations (Liu et al. 1999; Liu & Meyer-Hofmeister 2001). Further investigations show that the disk evaporation model can also interpret the hysteresis of accretion rate between the hard-to-soft transition and the soft-to-hard transition, which has been observed in quite a number of low-mass X-ray binaries (Meyer-Hofmeister et al. 2005; Liu et al. 2005). Recent studies

(Liu, Meyer, & Meyer-Hofmeister 2006; Meyer, Liu, & Meyer-Hofmeister 2007) show the disk evaporation model could explain the existence of an inner disk at intermediate states.

The original disk evaporation model was proposed by Meyer & Meyer-Hofmeister (1994), where the magnetic field is not included since the work aims at explaining the UV lag observed in dwarf novae. But magnetic field has long been realized to play an important role in accretion disks (SS73). Recently, observations also reveal the magnetic nature of disk accretion onto black holes (Miller et al. 2006). Meyer & Meyer-Hofmeister (2002) have included magnetic pressure in the disk evaporation model in order to explain the different truncation radii of the outer thin disks between the nuclei of elliptical galaxies and low luminosity AGN, which have similar Eddington-scaled accretion rate (normalized by the Eddington accretion rate $\dot{M}_{\text{Edd}} = L_{\text{Edd}}/\eta c^2$, where L_{Edd} is the Eddington luminosity, and η is the efficiency of energy conversion). One temperature model (hereafter 1-T, which means that the electrons and ions in the corona have the same temperature) was used in this previous study. Besides the contribution of the magnetic pressure to the total pressure, magnetic field can also affect the heat conduction. Meyer & Meyer-Hofmeister (2006) already took this effect into account together with the irradiation/Comptonization processes, and found that the variation of heat conduction can change the $\dot{m} - r$ relation significantly.

In this paper, we intend to investigate the influence of magnetic field on both the pressure and heat conduction in detail with a more realistic two temperature model (hereafter 2-T, which means that the electrons and ions in the corona have different temperatures, Liu et al. 2002a). We present more detailed numerical results and also give the fitting formula to the numerical results, which enables the comparison of theory and observations much easier. In §2 we briefly describe the model and basic equations; in §3 we present the numerical results; in §4 our results are compared with observations; in §5 we discuss the model itself and present our conclusions in §6.

2. Description of the model

Following previous works on disk evaporation (Meyer & Meyer-Hofmeister 1994; Liu, Meyer & Meyer-Hofmeister 1995; Meyer et al 2000a; Liu et al. 2002a), we pay our main attentions to the transition region between a SSD and a RIAF, which is characterized by a thin disk sandwiched by the corona flow. The viscous heat of ions is partially transferred to electrons by collisions and conducted down by electrons to the transition layer, which is cooler and denser. Part of the cool matter in the transition layer is heated and evaporated into the corona till an equilibrium density is reached. The gas in the corona carries similar angular momentum as that in the disk, and is continuously accreted to the central black

hole due to the viscous angular momentum transfer similar to that in accretion disks. The drifting-in gas is steadily re-supplied by the gas evaporating from the transition layer between the corona and the thin disk, and an equilibrium state of the system can be reached.

There are three factors crucial to the evaporation rate, i.e. the heating of the corona, the thermal conduction, and the radiative cooling in the transition layer. Any new physical process related to these three factors can influence the evaporation rate and eventually make the final configuration of the accretion flow different (e.g. Liu, Meyer & Meyer-Hofmeister 2005). One important relevant factor is the magnetic field because it has overall influence on accretion disks. Firstly, it enhances the viscosity (Balbus & Hawley 1991). Secondly, magnetic field contributes to the total pressure. The viscous heating changes by both the viscous coefficient and the pressure. Thirdly, strong entangled magnetic field largely modifies the heat conduction of the plasma (Tao 1995; Chandran & Cowley 1998; Narayan & Medvedev 2001). Fourthly, in the presence of magnetic field, there should be cyclotron-synchrotron radiation. In addition, magnetic dissipation/reconnection can be an additional heating mechanism to the corona.

However, how magnetic field influences the viscosity parameter α is still unclear. The contribution could already be included if α is as large as 0.3. The dependence of evaporation rate on the viscosity parameter has been discussed in Meyer-Hofmeister & Meyer (2001). Here we concentrate our investigations on the influences of magnetic pressure and heat conduction on the disk evaporation process. The cyclotron-synchrotron radiation is optically thick in our corona and could only be important when the electron temperature is higher than 10^9K , which is the case in the upper boundary layers. Compared with the cooling from heat conduction, the cooling from optically-thick synchrotron radiation in the upper layers can be neglected as long as the electron temperature is not too much higher than 10^9K , which is indeed the case in our computations (see also Meyer & Meyer-Hofmeister 2002). Thus, the cyclotron-synchrotron radiation will not be included in our calculations. For simplicity, we assume a chaotic magnetic field, which provides an isotropic magnetic pressure in the corona.

The basic equations and boundary conditions we adopted in this work are the same as those in Liu et al. (2002a), only with some minor changes. The viscosity parameter (SS73) is set to $\alpha = 0.3$. As having been shown in many previous works, the characteristics of disk evaporation are independent on the mass of central black hole, the results are the same for systems with stellar-mass and supermassive black holes. For clarity, we reproduce the basic equations here.

The mass continuity equation is:

$$\frac{d}{dz}(\rho v_z) = \eta_m \frac{2}{r} \rho v_r - \frac{2z}{r^2 + z^2} \rho v_z, \quad (1)$$

where ρ , v_z , v_r are the gas density, the vertical and radial component of the velocity, respectively. The factor η_m equals to 1 in the evaporation model (Meyer-Hofmeister & Meyer 2003).

The z-component of the momentum equation is:

$$\rho v_z \frac{dv_z}{dz} = -\frac{dP}{dz} - \rho \frac{GMz}{(r^2 + z^2)^{3/2}}, \quad (2)$$

where the total pressure P includes both the gas pressure P_g and the magnetic pressure P_m .

The equation of heat conduction is:

$$F_c = -\kappa T_e^{5/2} \frac{dT_e}{dz}. \quad (3)$$

where κ is the heat conduction coefficient, and T_e is the temperature of electrons.

The energy equation of ions is:

$$\begin{aligned} & \frac{d}{dz} \left\{ \rho_i v_z \left[\frac{v^2}{2} + \frac{\gamma}{\gamma - 1} \frac{P_i}{\rho_i} - \frac{GM}{(r^2 + z^2)^{1/2}} \right] \right\} \\ &= \frac{3}{2} \alpha P \Omega - q_{ie} + \eta_E \frac{2}{r} \rho_i v_r \left[\frac{v^2}{2} + \frac{\gamma}{\gamma - 1} \frac{P_i}{\rho_i} - \frac{GM}{(r^2 + z^2)^{1/2}} \right] \\ & - \frac{2z}{r^2 + z^2} \left\{ \rho_i v_z \left[\frac{v^2}{2} + \frac{\gamma}{\gamma - 1} \frac{P_i}{\rho_i} - \frac{GM}{(r^2 + z^2)^{1/2}} \right] \right\}. \end{aligned} \quad (4)$$

where v is the modulus of the velocity vector; ρ_i and P_i are the contribution of ions to the density and pressure, respectively; Ω is the angular velocity of the gas in the corona; q_{ie} is the heat transfer rate from ions to electrons due to the Coulomb coupling (Liu et al. 2002a), which can be expressed as

$$q_{ie} = \left(\frac{2}{\pi} \right)^{1/2} \frac{3}{2} \frac{m_e}{m_p} \ln \Lambda \sigma_T c n_e n_i (kT_i - kT_e) \frac{1 + T_*^{1/2}}{T_*^{3/2}}, \quad (5)$$

where m_e , m_p , T_i and T_e have their usual meaning; σ_T is the Thomson scattering cross section and $\ln \Lambda = 20$ is the Coulomb logarithm. $T_* = (kT_e/m_e c^2)(1 + (m_e/m_p)(T_i/T_e))$, γ is the ratio of specific heats, and k is the Boltzmann constant (rather than the heat conduction coefficient κ). The factor η_E equals to $\eta_m + 0.5$ (Meyer-Hofmeister & Meyer 2003).

The combined energy equation of ions and electrons is:

$$\begin{aligned}
 & \frac{d}{dz} \left\{ \rho v_z \left[\frac{v^2}{2} + \frac{\gamma}{\gamma - 1} \frac{P}{\rho} - \frac{GM}{(r^2 + z^2)^{1/2}} \right] + F_c \right\} \\
 &= \frac{3}{2} \alpha P \Omega - n_e n_i L(T_e) + \eta_E \frac{2}{r} \rho v_r \left[\frac{v^2}{2} + \frac{\gamma}{\gamma - 1} \frac{P}{\rho} - \frac{GM}{(r^2 + z^2)^{1/2}} \right] \\
 & \quad - \frac{2z}{r^2 + z^2} \left\{ \rho v_z \left[\frac{v^2}{2} + \frac{\gamma}{\gamma - 1} \frac{P}{\rho} - \frac{GM}{(r^2 + z^2)^{1/2}} \right] \right\}, \tag{6}
 \end{aligned}$$

where $\Lambda(T)$ is the radiative cooling function for a low-density, optically thin gas of cosmic abundances in the temperature range of $10^4 - 10^8$ K and is taken to be the Bremsstrahlung radiation function for $T > 10^8$ K (Raymond, Cox & Smith 1976).

Note that the last terms in the right side of Eq.(1), Eq.(4), and Eq.(6) are the flaring terms (Meyer & Meyer-Hofmeister 1994). The pressure P in these equations is no longer the gas pressure but the total pressure, so the sound speed (P/ρ) has an additional factor $1 + (1/\beta)$ compared with the sound speed without the magnetic pressure (P_g/ρ) (where $\beta \equiv P_g/P_m$ is the ratio of gas pressure to magnetic pressure). The ratio of specific heats γ also changes with β , with the relation $\gamma = (5\beta + 8)/(3\beta + 6)$ (cf. Appendix A of Esin 1997, but note that the definition of β is different there).

Both β and κ affect the lower boundary conditions in the corona, which are (Meyer-Hofmeister & Meyer 2006)

$$T_i = T_e = 10^{6.5} K, \tag{7}$$

$$F_c = -2.73 \times 10^6 P \lambda^{1/2} / (1 + \frac{1}{\beta}), \tag{8}$$

where $\lambda \equiv \kappa/\kappa_{\text{Sp}}$ is the fraction of the standard value (Spitzer value $\kappa_{\text{Sp}} = 10^{-6} g \text{ cm s}^{-3} K^{-7/2}$) of the heat conduction coefficient (Meyer-Hofmeister & Meyer 2006). We integrate Eq. (1) to Eq.(6) until the upper boundary conditions

$$v_z = c_s, \tag{9}$$

$$F_c = 0 \tag{10}$$

are fulfilled.

3. Numerical results

We consider chaotic magnetic fields and parameterize it by $\beta \equiv P_g/P_m$ (where $P_m \equiv B^2/24\pi$). So a smaller β value means stronger magnetic fields. Under an assumption of equipartition between the gas pressure and magnetic pressure, we have $\beta = 1$; MHD simulation yields $\beta \approx 12$ (Sharma et al. 2006); the case without magnetic field corresponds to $\beta = \infty$. Assuming different strength of magnetic pressure and heat conduction, we can numerically solve the vertical structure of the corona at different radii. Our main results are discussed as follows.

3.1. The vertical structure of the magnetized corona

Fig. 1 shows the vertical structure of the corona above a thin disk at a radius $R = 214R_S$. The left panel shows the structure without magnetic field, $\beta = \infty$ and $\kappa = \kappa_{Sp}$. The right panel shows the influence of the magnetic field on the structure with $\beta = 10/3$ and $\kappa = 0.5\kappa_{Sp}$. Comparing the two cases, we find that the vertical profile of the coronal quantities do not change much when magnetic field is included, though the absolute values, for example, the density and evaporation rate, do change. This is a typical feature in the disk corona also shown in earlier works (e.g. Meyer et al 2000a), which indicates that the corona above a thin disk undergoes very steep changes in temperature, density, and can not be simply averaged in the vertical direction.

3.2. The meaning of $\dot{m} - r$ curve

Qualitatively similar to previous results (Meyer et al. 2000a; Liu et al. 2002a), our new calculations with the magnetic field show that the mass evaporating from the disk to the corona increases toward the central black hole, reaching a maximum at a few hundred Schwarzschild radii and dropping very quickly near the black hole. The distribution of the evaporation rate along the distance turns out to be independent on the black hole mass. We scale the evaporation rate by the Eddington accretion rate $\dot{M}_{Edd} \equiv L_{Edd}/0.1c^2 = 1.39 \times 10^{18} M/M_\odot$, then $\dot{m} \equiv \dot{M}/\dot{M}_{Edd}$, and scale the distances by Schwarzschild radius $R_S = 2GM/c^2$, then $r \equiv R/R_S$. We will show the dependence of \dot{m} on r so that the relations $\dot{m}(r)$ can be tested by observations on some black hole X-ray binaries.

The $\dot{m} - r$ curve can predict the configuration of accretion flow at different accretion rates. If the mass accretion rate of accretion disk is lower than the maximal evaporation rate, the disk will be depleted inside a radius where the accretion rate equals to the evaporation

rate. This truncation radius is outside the radius of the maximal evaporation rate. The accretion flow is then dominated by an inner pure corona, or more exactly, the ADAF/RIAF. Such a configuration corresponds to the low/hard spectral state in black hole X-ray binaries. However, it is also possible that there is an inner disk which is separated from the outer disk by a 'pure corona flow' if the accretion rate is close to the maximal evaporation rate (Liu et al. 2006). This configuration is thought to be related to the intermediate spectral state. If the mass accretion rate exceeds the maximal evaporation rate, the disk cannot be depleted anywhere, so it can extend to the marginal stable radius (Meyer et al. 2000a). The radiation is dominantly from the standard thin disk and the corona is suppressed by the Compton cooling. This situation corresponds to the high/soft spectral state.

The change of mass accretion rate in the disk can also cause the transition between different spectral states. As an example, if the mass accretion rate in the disk increases from a value smaller than the maximal (critical) evaporation rate to a value larger than that, a hard-to-soft state transition would occur, and vice versa. So the maximal evaporation rate corresponds to a transition accretion rate (or a transition luminosity). This transition accretion rate and the truncation radius of the disk in the low/hard, as shown in our predicted $\dot{m} - r$ curves, are the two parameters to be compared with the observational results.

3.3. The influence of magnetic field on $\dot{m}(r)$

We investigate the influence of magnetic pressure by calculating the evaporation rate for a series of β values. Our results based on both 1-T model and 2-T model are present in the $\dot{m} - r$ curves.

The $\dot{m} - r$ relation of 1-T model is shown in Fig. 2. The solid line, the dot-dashed line, and the long-dashed line represent the cases of $\beta = \infty$ (no magnetic field), $\beta = 5$, and $\beta = 2$ respectively. We didn't calculate the curves with even smaller β , since magnetic field would be too strong in those cases, invalidating the assumptions of our current model. The most obvious changes by the inclusion of magnetic field happen to the value and location of the maximal evaporation rate. From Fig. 2 we see that in the 1-T model, the maximal evaporation rate increases with the increase of magnetic field, while its location moves inward. This can be understood as a consequence of the enhanced viscous heating due to the contribution of magnetic pressure. The viscous heat cannot be efficiently consumed by radiative cooling until a higher density is reached in the inner region. There is also another influence lying in the outer region (at large radii) of the corona. In contrast to the maximal evaporation rate, the evaporation rate at a fixed radius increases with the decrease of magnetic field. This is because that the viscous heating is balanced by the advection rather

than by radiation in the outer region of the corona. The viscous heating contributed by the magnetic pressure is mainly transferred to enthalpy of gas which makes the gas hotter than the case without magnetic field and hence radiative cooling is more efficient if the density is unchanged. This leads to a reduced evaporation rate. These trends are consistent with the qualitative estimations given by Meyer et al. (2000a) (See their Eq. (56) and Eq. (57)). These evaporation features are basically relying on enhanced dissipation rate produced by the enhanced magnetic pressure, which might be true in other dissipation models as well, including those based on reconnection and shocks in a strongly magnetized corona.

Such a distribution of evaporation rate along distance, as shown in Fig. 2, implies that at a given accretion rate the truncation of disk occurs at smaller radius with the involving of magnetic field and the disk can extend to a smaller radius before the system transits to the soft state.

In the 2-T model we take into account the decoupling of electrons and ions probably occurring in the inner region. When electrons and ions are decoupled, the electron heating by collision with ions is inefficient. A large fraction of heat is stored in ions and the heat to evaporate the gas in the disk is thus limited. Therefore, a smaller evaporation rate is expected in the 2-T scenario than that in the 1-T case, especially in the inner region. Our numerical results are shown in Fig. 3. The lines other than the short-dashed line represent the results calculated for the 2-T model, with the same notations as in Fig. 2 for the 1-T model. As expected, the 1-T results and 2-T results are similar in the outer region. However, there are clear differences in the inner region where ions and electrons are not well coupled. Because the 2-T model usually describes the real physics in the inner hot accretion flow, we will concentrate our discussion on the 2-T model. Fig. 3 shows that the curve for evaporation rate shifts inwards with the increase of magnetic field, while the maximal evaporation rates keep more or less the same, around 2-3% of the Eddington rate. This indicates that the involve of magnetic field results in a smaller truncation radius of the thin disk. The stronger the magnetic field is, the smaller radius the disk is truncated at. However, our result implies that the transition from the hard state to the soft state occurs at almost the same accretion rate, no matter the magnetic field is included or not. Such a feature may interpret why some objects truncate at smaller radius than that predicted by previous models (see section 4). To show more detailed influence of magnetic field we list the maximum evaporation rates and the corresponding radii for different β values in the upper part of Table 1. The data can be linearly fitted by $\log \dot{m}_{\max} = 0.143/\beta - 1.579$ and $\log r_{\max} = -1.750/\beta + 2.299$.

3.4. The influence of heat conduction $\dot{m}(r)$

Theoretical works have shown that the chaotic magnetic field would suppress the heat conduction in the plasma (Tao 1995; Chandran & Cowley 1998; Narayan & Medvedev 2001). Recent work reports that the coefficient of heat conduction can be reduced to one fifth of the Spitzer value (Narayan & Medvedev 2001). We calculate the $\dot{m} - r$ relation for different κ with both the 2-T model and 1-T models. The 2-T results do not include the irradiation/Comptonization effects since we are more interested in the influence caused by the heat conduction. The hard radiations from the inner corona/ADAF can heat up electrons (irradiation) in most of the corona region whereas cool electrons (Comptonization) in the innermost region, thereby lead to an outward shift of the evaporation curve $\dot{m}(r)$ (Liu et al. 2005), counteracting partially the effect of reduced heat conduction. For details of the combined effect of heat conduction and irradiation/Comptonization one can refer to the work of Meyer-Hofmeister & Meyer (2006).

Fig. 4 shows the dependence of the $\dot{m} - r$ relation on κ based on the 2-T model. The solid line represents the standard case with $\kappa = \kappa_{\text{Sp}}$. The dot-dashed line and the long-dashed line correspond to $\kappa = 0.5\kappa_{\text{Sp}}$, and $\kappa = 0.2\kappa_{\text{Sp}}$, respectively. For comparison, a curve with $\kappa = \kappa_{\text{Sp}}$ in the 1-T model is also shown as a short-dashed line. Fig. 4 looks very similar to Fig. 3. The location of the maximal evaporation rate moves inward with the decrease of κ , but the maximal evaporation rate is insensitive to κ . Detailed values of our calculation and the corresponding linearly fitting results are listed in the lower half of Table 1. Comparing the fitting results for both the cases of magnetic pressure and heat conduction, we find that the influence of magnetic field is much stronger than that of the heat conduction. Note that the chaotic magnetic field tends to decrease the heat conduction by deflecting the motion of electrons and the inclusion of magnetic field would greatly reduce the disk truncation radius through both β and κ . We'll show a composite result in the next subsection.

The 1-T results with different κ values are plotted in Fig. 5, which shows the similar tendency as the influence of β . Due to the decoupling of electrons and ions in the inner region, the 1-T results are less meaningful than the 2-T results.

3.5. The combined effect of β and κ

Qualitatively the presence of chaotic magnetic field can reduce the efficiency of heat conduction by electrons. But how κ changes with β remains unclear. As an example, we take $1/\beta = 0.3$ and $\kappa = 0.5\kappa_{\text{Sp}}$ to calculate the evaporation rates at different radii. The results are shown in Fig. 6 (the dotted line). One can see that the magnetic pressure

and the heat conduction play similar roles to the shift of $\dot{m}(r)$. That is, the increase of magnetic field or the decrease of heat conduction shifts the evaporation curve $\dot{m}(r)$ inwards. Their combined effects are the superposition of the shifts caused separately by the magnetic pressure and the heat conduction. However, the maximal evaporation rate increases slightly with magnetic pressure and even more slightly with heat conduction. Since the magnetic field tends to reduce the efficiency of heat conduction, the two effects on the maximal evaporation rate counteracts each other in the case of the inclusion of magnetic field, thereby keeping the maximal rate almost constant. The maximal evaporation rate influenced by the combination of β and κ can be derived roughly from the combined linear fitting to the two sets of data together with the data from the case of ($\beta = 0.3$, $\kappa/\kappa_{\text{Sp}} = 0.5$), namely,

$$\log \dot{m}_{\text{max}} = 0.101/\beta + 0.023\kappa/\kappa_{\text{Sp}} - 1.589, \quad (11)$$

$$\log \dot{m}_{\text{max}} = -0.272 \log \beta' + 0.037 \log(\kappa/\kappa_{\text{Sp}}) - 1.566, \quad (12)$$

where $\dot{m}_{\text{max}} = \dot{M}_{\text{max}}/\dot{M}_{\text{Edd}}$ and $\beta' = \beta/(\beta + 1)$.

The location of the maximal evaporation rate can be obtained in the same way, namely,

$$\log r_{\text{max}} = -1.935/\beta + 0.899\kappa/\kappa_{\text{Sp}} + 1.466, \quad (13)$$

$$\log r_{\text{max}} = 5.158 \log \beta' + 1.170 \log(\kappa/\kappa_{\text{Sp}}) + 2.333, \quad (14)$$

where $r_{\text{max}} = R_{\text{max}}/R_{\text{S}}$.

Eqs.(11) to (14) show more clearly than Fig. 6 that the maximal evaporation rate hardly changes with the inclusion of magnetic field and heat conduction; while the truncation radius depends strongly on both the magnetic pressure and heat conduction. This implies, if there exists magnetic field in the disk, the truncation of the disk could occur at much smaller radii, while the hard-to-soft state transition should occur at more or less the same accretion rate, $\dot{m} \approx 0.03$. For instance, in the case of $1/\beta = 0.3$, $\kappa = 0.5\kappa_{\text{Sp}}$ (shown by the dotted line in Fig. 6), the hard/soft transition occurs at $\dot{m} = 0.028$ and the disk can extend down to $\sim 27R_{\text{S}}$ before the transition. Such a transition radius is much smaller than the prediction of $\sim 209R_{\text{S}}$ without involving the magnetic field.

If the dependence of κ on magnetic field is known, we can more accurately determine the maximal evaporation rate and the corresponding radius, and make the comparison of the theoretical predictions with the accretion rate and inner disk radius determined by observations during the hard-to-soft state transition.

4. Comparison of the model predictions with Observations

Our numerical results can be compared with observations. Since the results predicted by the disk evaporation model are mass scale-free, they can be used in various systems with different masses of central black holes.

4.1. Luminosities at spectral state transitions in X-ray binaries

The maximal evaporation rate in the $\dot{m} - r$ curve predicts a critical accretion rate at which a transition occurs between the hard and soft spectral states. When the accretion rate in the disk is lower than the critical one, the evaporation depletes the disk and the accretion flow is eventually replaced by an ADAF/RIAF. When the accretion rate is higher than the critical value, the standard thin disk can extend down to the last stable orbit and thus dominates the accretion flows. From Fig. 3 and Fig. 4, one can see that this transition accretion rate is around $0.03\dot{M}_{\text{Edd}}$ on the basis of the 2-T model (the 1-T model gives $0.02\dot{M}_{\text{Edd}}$, see also Meyer et al. 2000a), which is weakly dependent on the strength of magnetic pressure and heat conduction. This quantity can be compared with the transition luminosities in black hole X-ray binaries if the efficiency of energy conversion η is similar.

The observed transition luminosities (scaled by the Eddington luminosity) in some black hole X-ray binaries are listed in Table 2. One can see that different objects have transition luminosities ranging from 1% to 15%. The average value of the transition luminosities is 0.036. However, when we talk about the transition luminosities, we must take special cautions. Firstly, the luminosities of different sources are observed at different energy band and may not represent the bolometric luminosities. Secondly, these observation values of transition luminosities suffer from the uncertainties of some parameters, such as the masses of the central black holes and the source distances (Gierliński & Newton 2006). If these dimensionless transition luminosities can represent the corresponding dimensionless mass accretion rates, we can estimate their average value as 0.036. This value predicted by the disk evaporation model (~ 0.03) is well consistent with the observational result.

4.2. Truncation radius and the corresponding accretion rate at hard states

In the hard state of black hole X-ray binaries, the accretion rate in the disk is lower than the maximal evaporation rate, and the thin disk will be truncated at a radius where the accretion rate in the disk equals to the evaporation rate. So the $\dot{m} - r$ relation can be tested by the truncation radius of the disk and the corresponding accretion rate estimated

from the observational data.

For such a purpose, we collect some data from black hole X-ray binaries (see Table 3). These data are based on the spectral fitting with the ADAF + disk model (Narayan, Barret & McClintock 1997). The accretion rates in Table 3 are the Eddington-scaled values ($\dot{m} = 0.1\dot{M}c^2/L_{\text{Edd}}$), which are converted from the Eddington ratios (L/L_{Edd}) (Zdziarski et al. 2004), or from the rates scaled by the critical accretion rate ($\dot{m} \equiv \dot{M}c^2/L_{\text{Edd}}$, Wilms et al. 1999), or from \dot{M} (in the unit of solar mass per year) (Poutanen et al. 1997). The data listed in Table 3 can then be compared with the theoretical results from our model.

Fig. 7 shows the observational data together with our model predictions for different strength of magnetic pressure and heat conduction. One can see that the enhanced magnetic pressure and reduced heat conduction bring the model predictions much closer to the observations. We expect that theoretical results with stronger magnetic field or further reduced heat conduction or both will predict more consistent results with observations. Here we don't give such an example not only because we don't know the accurate strength of magnetic field in individual objects, but also due to the large uncertainties in the observational data. Caution should be taken here that there are several sets of data given in the original papers, we just listed the best fitted ones here. We also noticed that in modeling the low-state spectrum of XTE J1118+480 by an inner ADAF and an outer disk (Esin et al. 2001), the ratio $P_g/(P_g + P_m)$ in the ADAF is set to 0.97, which corresponds to $\beta = 32$ in this work.

5. Discussion

5.1. Comparison with earlier estimations

Our 1-T calculations confirm the results estimated by Meyer et al. (2000a), namely,

$$\left(\frac{\dot{M}}{\dot{M}_{\text{Edd}}}\right) \propto \frac{\alpha^3}{\kappa^{1/2}} \left(1 + \frac{1}{\beta}\right)^{5/2}, \quad (15)$$

$$\left(\frac{R}{R_{\text{S}}}\right) \propto \frac{\kappa}{\alpha^2} \left(1 + \frac{1}{\beta}\right)^{-4}. \quad (16)$$

However, our results from the 2-T model are different from that of the 1-T model. The maximal evaporation rate remains almost the same with the decrease of both β and κ , though the location of maximal evaporation rate moves to smaller radii in a similar way to that in the 1-T model. In the outer region, both the 2-T model and the 1-T model give similar results, since the accretion flow is close to a 1-T flow. However, in the inner region,

ions and electrons are decoupled. The accretion energy is mainly stored in the ions and the temperature of ions is higher than that of electrons. Therefore, the accretion flow is a 2-T flow. There is little heat conducted by the electrons from corona to the disk, and thus the matter evaporation is inefficient compared to the 1-T case.

5.2. Cooling by cyclo-synchrotron radiation

With the inclusion of magnetic field, one potential cooling mechanism is the cyclo-synchrotron radiation, which is negligible in the lower layers (Meyer & Meyer-Hofmeister 2002). In the highest part of the corona, it may influence the temperature (one can refer to the discussion of synchrotron radiation in Narayan & Yi (1995) and Mahadevan (1997)). However, we expect little influence from cyclo-synchrotron radiation on the main body of the coronal action.

5.3. Heating by magnetic field dissipation

Besides the influence on some physical processes such as heat conduction, the magnetic field may play an important role in the formation of corona (Galeev, Rosner & Vaiana 1979). Disk magnetic fields rising into the corona contain energy that originates in the disk accretion but will be dissipated (e.g. by reconnection and shocks) in the corona. We take this very roughly into account by scaling the viscous dissipation in our modeling to the total instead to the gas pressure and thus including parts which are related to the addition of disk produced magnetic flux that raise the magnetic pressure, i.e. lead to a lower beta in the corona.

5.4. Comparison with MHD simulation

Detailed investigations on the formation of a magnetized corona from MHD simulation (e.g. Miller & Stone 2000; Hawley & Balbus 2002; Machida, Hayashi, & Matsumoto 2000) show that a strongly magnetized corona can form above an initially weakly magnetized disk. Miller & Stone (2000) showed that magnetic field is amplified within 2 disk scale height ($H=0.01R$) and the energy is mostly dissipated in 3 to 5 scale height, thereby heats up the corona. Machida et al. (2000) also showed that a low- β corona in the form of "patch corona" or active coronal region. More recent work (Hirose, Krolik, & Stone 2006), which includes radiation transport, shows that magnetic dominance happens deeper than the photosphere, where the medium is still relatively cool. Here we consider a slab corona in a large vertical

extent where the structure is vertically stratified, in contrast to an isothermal torus in the MHD simulation. More importantly, the vertical thermal conduction is taken into account in our model. This leads to efficient mass evaporation from the disk to the corona, feeding a corona to higher mass density than that in the coronal envelope shown in MHD simulations. Therefore, we expect relatively higher β value in our case.

6. Conclusion

We investigate the influence of coronal magnetic fields on the structure of an accretion disk corona sustained by dissipative energy release and thermal coupling between corona and disk. Numerical calculations show that the relation between mass evaporation rate and radius (\dot{m} - r curve) systematically shifts to smaller radii with both an increase of magnetic pressure (decreasing β) and a decrease of heat conductivity (decreasing κ). The location of maximal evaporation rate lies between $30R_S$ and $200R_S$ when β ranges from 2 to ∞ or κ from κ_{Sp} to $0.2\kappa_{Sp}$. However, the maximal evaporation rate remains almost the same ($\sim 0.03\dot{M}_{Edd}$, with energy conversion efficiency $\eta = 0.1$) If the disk truncation and state transition are indeed caused by an evaporation process, the transition luminosity predicted by our disk evaporation model is $L_{tr} = 0.03L_{Edd}$ before transition to the soft state. The inner edge of the outer thin disk can be several ten to several hundred Schwarzschild radii, depending on the strength of magnetic field and its effect on the heat conduction. This alleviates the problem that the previous evaporation models predict too large a disk truncation radius before the transition from hard to soft state. Our predictions with the inclusion of the coronal field are found to be in better agreement with the observational results of several black hole X-ray binaries, though discrepancies remain.

We thank F. Meyer and E. Meyer-Hofmeister for detailed discussions on the computational results and for their reading through the manuscript and comments on it. We also thank F.K. Liu for helpful discussions. Q.L. wishes to thank the hospitality of High Energy Astronomy Group at YNAO, which makes this work possible. This work is partially supported by the National Natural Science Foundation of China (Grants-10533050, 10473001, 10525313), the BaiRenJiHua program of the Chinese Academy of Sciences, and the RFDP (Grant 20050001026).

REFERENCES

Balbus, S. A., & Hawley, J. F. 1991, ApJ, 376, 214

- Chandran, B. D. G., & Cowley, S. C. 1998, *Phys. Rev. Lett.*, 80, 3077
- Esin, A. A., McClintock, J. E., & Narayan, R. 1997, *ApJ*, 489, 865
- Esin, A. A. 1997, *ApJ*, 482, 400
- Esin, A. A. et al. 2001, *ApJ*, 555, 483
- Galeev, A. A., Rosner, R. & Vaiana, G. S. 1979, *ApJ*, 229, 318
- Gierliński, M. & Newton, J. 2006, *MNRAS*, 370, 837
- Hameury, J.-M. et al. 1997 *ApJ*, 489, 234
- Hawley, J. F. & Balbus, S. A. 2002, *ApJ*, 573, 738
- Hirose, S., Krolik, J. H., & Stone, J.M. 2006, *ApJ*, 640, 901
- Honma, F. 1996 *PASJ*, 48, 77
- Liu, B. F. et al. 1999 *ApJ*, 527, L17
- Liu, B. F. & Meyer-Hofmeister 2001 *A&A*, 372, 386
- Liu, B. F., Mineshige, S., Meyer, F., Meyer-Hofmeister, E., & Kawaguchi, T., 2002a, *ApJ*, 575, 117
- Liu, B. F., Mineshige, S., & Shibata, K. 2002b, *ApJ*, 572, L173
- Liu, B. F., Meyer, F., & Meyer-Hofmeister, E. 2005 *A&A*, 442, 555
- Liu, B. F., Meyer, F., & Meyer-Hofmeister, E. 2006 *A&A*, 454, L9
- Liu, F. K., Meyer, F., & Meyer-Hofmeister, E. 1995 *A&A*, 300, 823
- Lu, J. F., Lin, Y. Q., & Gu, W. M. 2004 *ApJ*, 575, 117
- Maccarone, T. J. 2003, *A&A*, 409, 697
- Machida, M., Hayashi, M. R., Matsumoto, R. 2000, *ApJ*, 532, L67
- Mahadevan, R. 1997, *ApJ*, 477, 585
- Mayer, M. & Pringle, J. E., 2007, *MNRAS*, 376, 435
- Meyer, F., & Meyer-Hofmeister, E. 1984 *A&A*, 132, 143

- Meyer, F., & Meyer-Hofmeister, E. 1994 A& A, 288, 175
- Meyer, F., Liu B. F., & Meyer-Hofmeister, E. 2000a A& A, 361, 175
- Meyer, F., Liu B. F., & Meyer-Hofmeister, E. 2000b, A& A, 354, L67
- Meyer, F., & Meyer-Hofmeister, E. 2002, A&A, 392, L5
- Meyer, F., Liu, B.F., & Meyer-Hofmeister, E. 2007, A&A, 463, 1
- Meyer-Hofmeister, E. , & Meyer, F. 2003, A&A, 420, 1013
- Meyer-Hofmeister, E. Liu, B. F., & Meyer, F. 2005, A&A, 432, 181
- Meyer-Hofmeister, E. & Meyer, F. 2006, A&A, 449, 443
- Miller, J. M. et al. 2006, Nature, 441, 953
- Miller, K. A., & Stone, J. M., 2000, ApJ, 534, 398
- Mushotzky, R. F., Done, C., & Pounds, K. A. 1993, ARA&A, 31, 717
- Narayan, R., & Yi, I. 1994, ApJ, 428L, 13
- Narayan, R., & Yi, I. 1995, ApJ, 452, 710
- Narayan, R., Barret, D., & McClintock, J. E. 1997, ApJ, 482, 448
- Narayan, R., & Medvedev, M. V. 2001, ApJ, 562, L129
- Poutanen, J., Krolik, J. H., & Ryde, F. 1997, MNRAS, 292, L21
- Pringle, J. E. 1981, ARA&A, 19, 137
- Quataert, E., di Matteo, T., Narayan, R., & Ho, L. C. 1999, ApJ, 525, 89
- Raymond, J. C., Cox, D. P., & Smith, B. W. 1976, ApJ, 204, 290
- Rees, M. J. 1984, ARA&A, 22, 471
- Remillard, R. A. & McClintock, J. E. 2006, ARA&A, 44, 49
- Shakura, N. I., & Sunyaev, R. A. 1973, A& A, 24, 337
- Sharma, P., Hammet, W., Quataert, E. et al. 2006, ApJ, 637, 952
- Shmeleva, O. P., & Syrovatskii, S. L. 1973, Sol. Phy., 33, 341

Tao, L. 1995 MNRAS, 275, 965

Wilms, J. et al. 1999, ApJ, 522, 460

Yuan, F., Quataert, E., & Narayan, R. 2003, ApJ, 598,301

Zdziarski, A. A. et al. 2004, MNRAS, 351, 791

Table 1: Influences of magnetic pressure and heat conduction on the maximal evaporation rate and its radius, followed by the best linear fitting results

$1/\beta$ ($\kappa/\kappa_{\text{Sp}} = 1.0$)	$\log \beta' = \log(\beta/(\beta + 1))$	$\log(R_{\text{max}}/R_{\text{S}})$	$\log(\dot{M}_{\text{max}}/\dot{M}_{\text{Edd}})$
0.0	0.000	2.320	-1.575
0.1	-0.041	2.110	-1.579
0.2	-0.079	1.920	-1.544
0.3	-0.114	1.780	-1.530
0.4	-0.146	1.615	-1.520
0.5	-0.176	1.420	-1.513
<hr/>			
$\log(R_{\text{max}}/R_{\text{S}}) = -1.750/\beta + 2.299$			
$\log(\dot{M}_{\text{max}}/\dot{M}_{\text{Edd}}) = 0.143/\beta - 1.579$			
$\log(R_{\text{max}}/R_{\text{S}}) = 4.971 \log \beta' + 2.321$			
$\log(\dot{M}_{\text{max}}/\dot{M}_{\text{Edd}}) = -0.408 \log \beta' - 1.581$			
$\kappa/\kappa_{\text{Sp}}$ ($1/\beta = 0.0$)	$\log(\kappa/\kappa_{\text{Sp}})$	$\log(R_{\text{max}}/R_{\text{S}})$	$\log(\dot{M}_{\text{max}}/\dot{M}_{\text{Edd}})$
0.2	-0.699	1.540	-1.600
0.5	-0.301	1.990	-1.561
0.6	-0.222	2.070	-1.561
0.7	-0.155	2.160	-1.563
0.8	-0.097	2.200	-1.567
0.9	-0.046	2.290	-1.571
1.0	0.000	2.320	-1.575
<hr/>			
$\log(R_{\text{max}}/R_{\text{S}}) = 0.956\kappa/\kappa_{\text{Sp}} + 1.440$			
$\log(\dot{M}_{\text{max}}/\dot{M}_{\text{Edd}}) = 0.024\kappa/\kappa_{\text{Sp}} - 1.588$			
$\log(R_{\text{max}}/R_{\text{S}}) = 1.124 \log(\kappa/\kappa_{\text{Sp}}) + 2.325$			
$\log(\dot{M}_{\text{max}}/\dot{M}_{\text{Edd}}) = 0.040 \log(\kappa/\kappa_{\text{Sp}}) - 1.563$			

Table 2: Transition luminosity in black hole X-ray binaries

Source	L_{trans}/L_E	Ref.
Nova Mus 91	0.031	1
XTE J 1550-564	0.034	1
GS 2000+251	0.0069	1
Cyg X-1	0.028	1
GRO J 1655-40	0.0095	1
LMC X-3	0.014	1
XTE J 1550-564	0.03	2
XTE J 1650-500	0.02	2
XTE J 2012+381	0.02	2
4U 1543-47	0.07	2
GX 339-4	0.15 or 0.05	2
GX 339-4	0.06 or 0.02	2
GX 339-4	0.14	3
$\sum_{i=1}^n L_i/n$	0.036	

Reference: 1. From Maccarone (2003). Note: the luminosities of different sources are at different energy bands. 2. From Gierliński & Newton (2006). Note: the luminosity is in the 1.5-12 keV band. 3. From Zdziarski et al. (2004).

Table 3: Accretion rates and truncation radii of disk determined from observations

Source	R_{in}/R_S	\dot{m} ^a	Reference
GX 339-4	200	0.005	Wilms et al. 1999
GX 339-4	100	0.008	Wilms et al. 1999
GX 339-4	10 ~ 100	0.015 ~ 0.07	Zdziarski et al. 2004
GRO J1655-40	1000	0.0034 ~ 0.0037	Hameury et al. 1997
XTE J1118+480	55	0.02	Esin et al. 2001
Cyg X-1	20	0.023	Poutanen et al. 1997

^a These accretion rates are scaled by $\dot{M}_{\text{Edd}} \equiv L_{\text{Edd}}/\eta c^2$ with $\eta = 0.1$, namely $\dot{m} = \dot{M}/\dot{M}_{\text{Edd}}$.

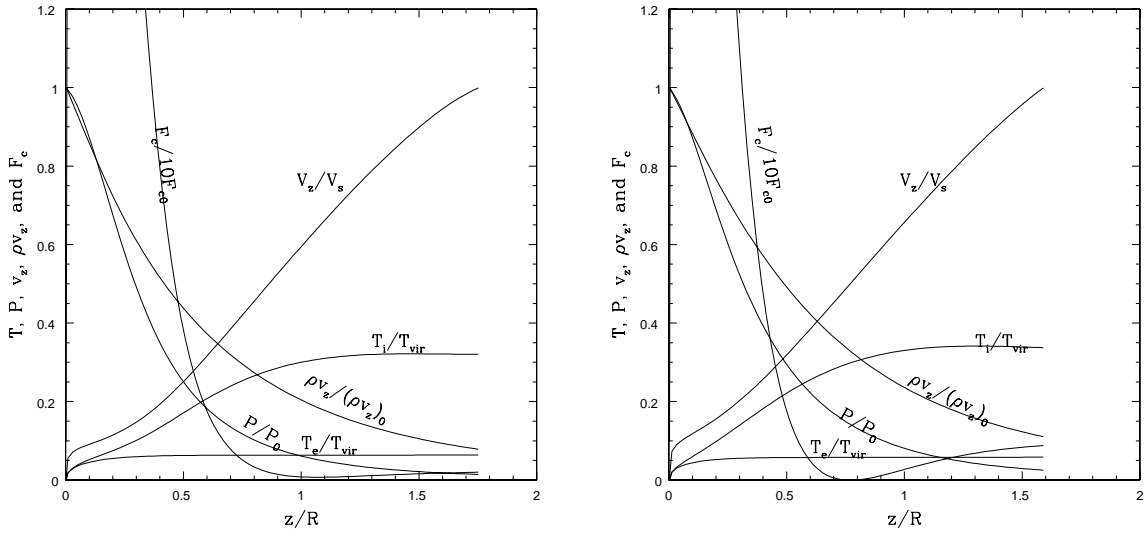


Fig. 1.— This figure shows the vertical structure of the corona around a black hole at a distance $R/R_S = 214$. z is the height above the equatorial plane of the accretion flow. T_e and T_i are electron temperature and ion temperature, respectively, while T_{vir} is the virial temperature used for scale. F_c , ρv_z , P , and v_z are the heat flux, vertical mass flow rate per unit area, total pressure, and vertical velocity, respectively. v_s is the sound speed used for scale. The quantities with subscript 0 are the values at the lower boundary. Left: no magnetic field, $\beta = \infty$ and $\kappa = \kappa_{SP}$. Right: With magnetic field, $\beta = 10/3$ and $\kappa = 0.5\kappa_{SP}$.

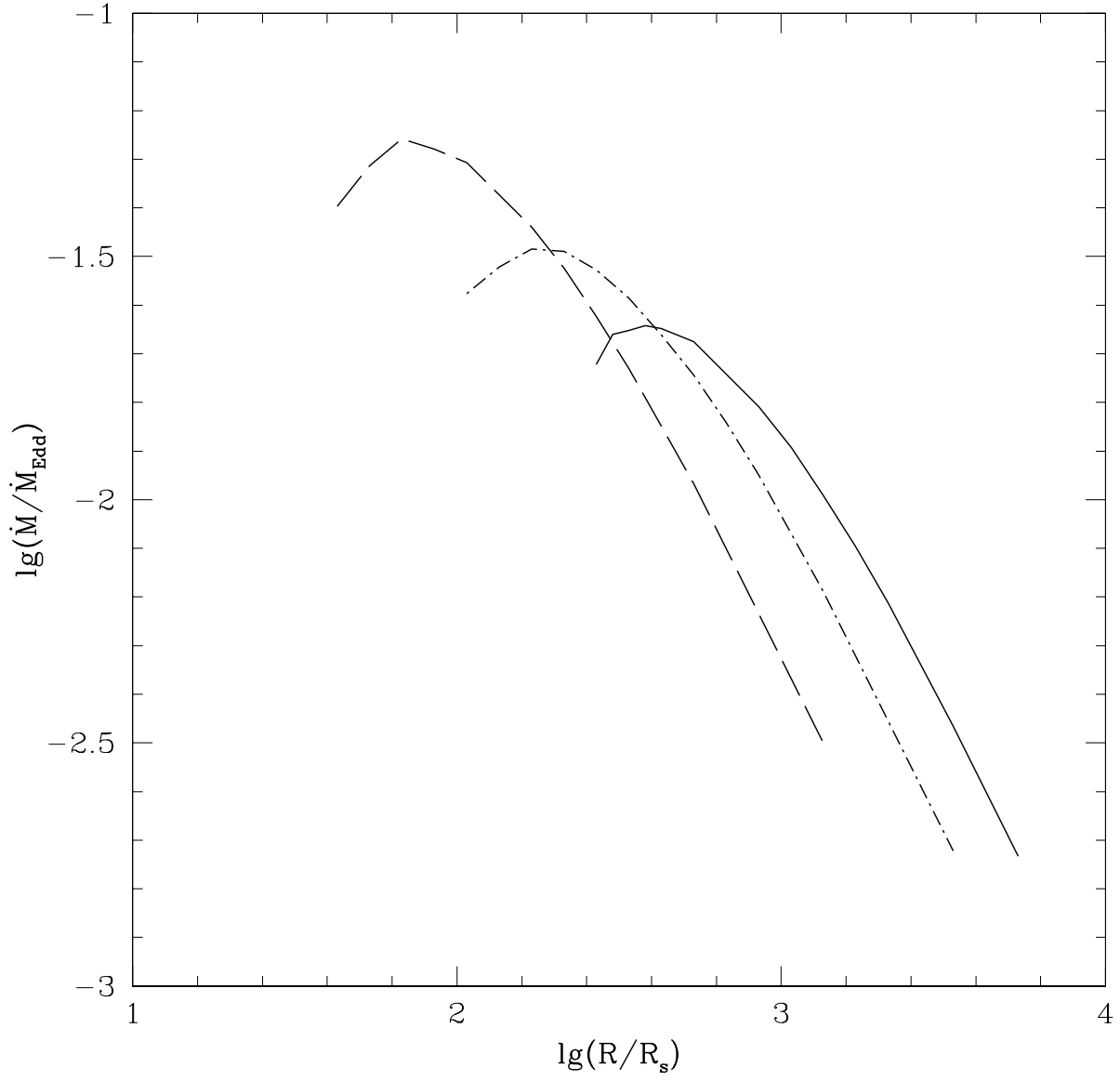


Fig. 2.— The $\dot{m} - r$ relation for different β values in the 1-T model. The solid line, dash-dotted line, and long-dashed line represent the cases of $\beta = \infty$, $\beta = 5$, and $\beta = 2$ respectively. The decrease of β value corresponds to the increase of magnetic field strength.

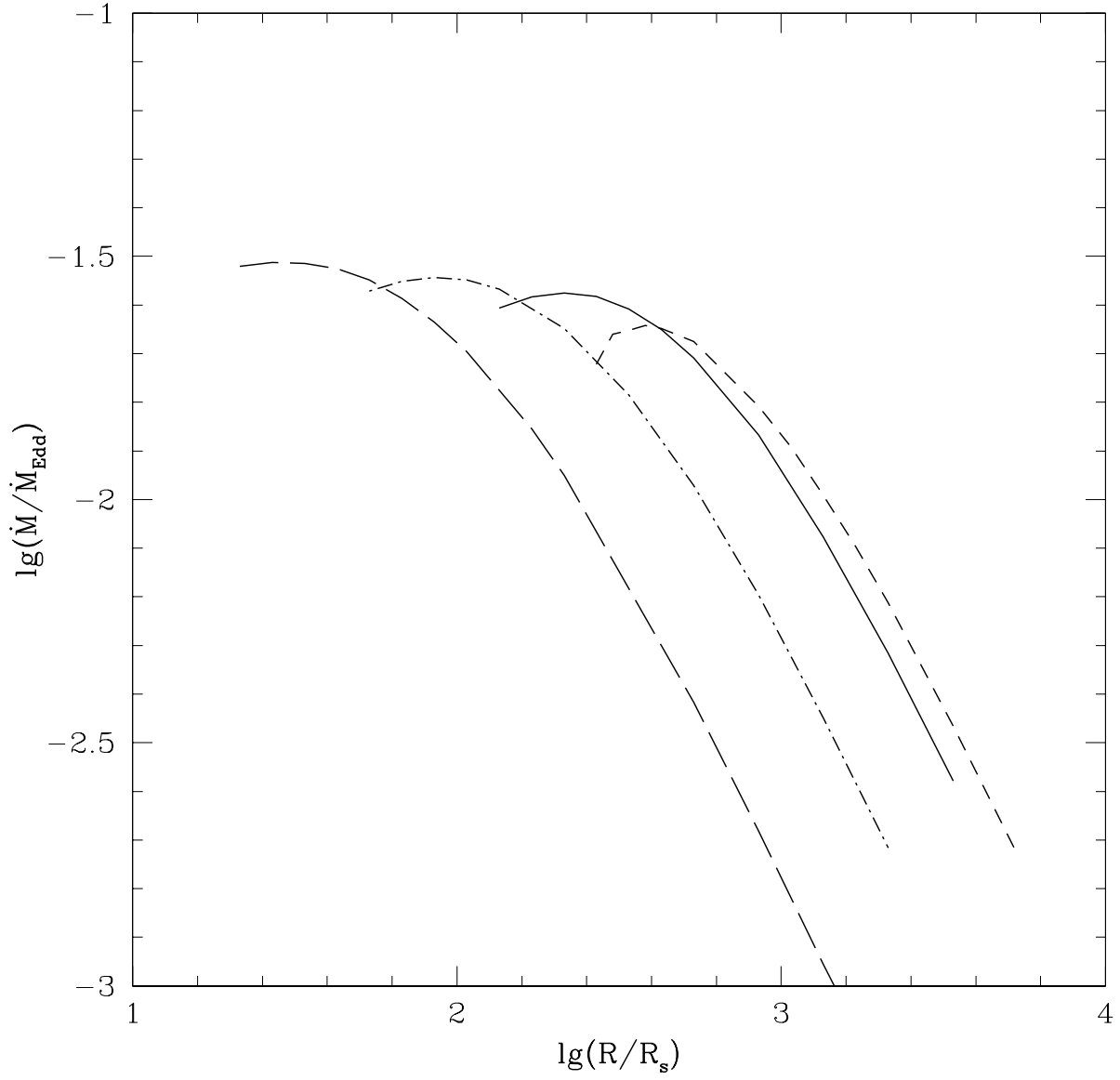


Fig. 3.— The $\dot{m} - r$ relation for different β values in the 2-T model. The short-dashed line represents the case of $\beta = \infty$ in the 1-T model, which is plotted here for comparison. Other lines represent the curves in the 2-T model. The solid line, dot-dashed line, and long-dashed line represents the cases of $\beta = \infty$, $\beta = 5$, and $\beta = 2$ respectively.

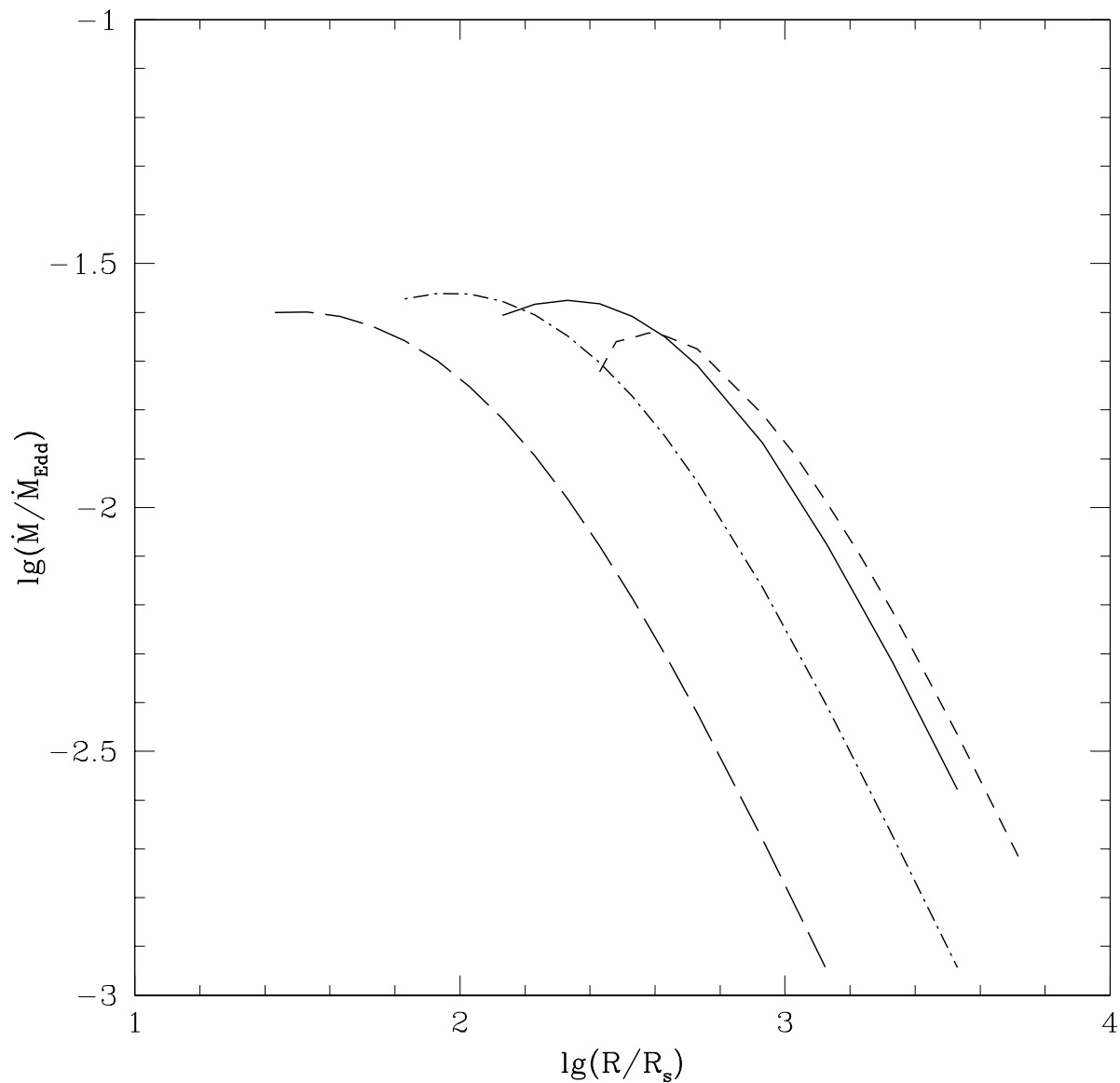


Fig. 4.— The $\dot{m} - r$ relation for different κ values in the 2-T model. The short-dashed line is for $\kappa = \kappa_{\text{Sp}}$ of the 1-T model and is plotted here for comparison. The solid line, dot-dashed line, and long-dashed line represent the cases of $\kappa = \kappa_{\text{Sp}}$, $\kappa = 0.5\kappa_{\text{Sp}}$, and $\kappa = 0.2\kappa_{\text{Sp}}$, respectively.

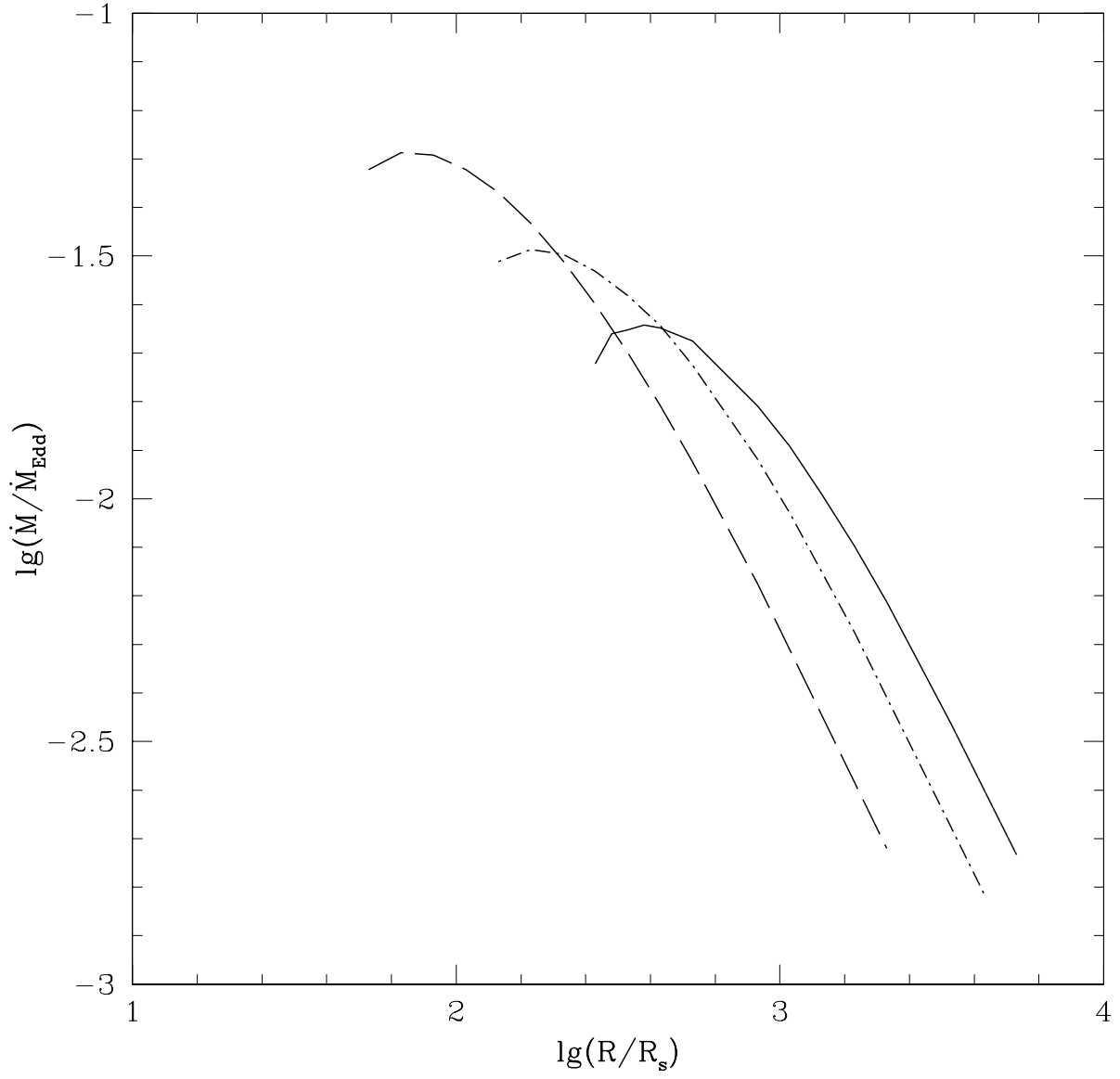


Fig. 5.— The $\dot{m} - r$ relation for different κ values in the 1-T model, The solid line, dot-dashed line, and long-dashed line represent the cases of $\kappa = \kappa_{\text{SP}}$, $\kappa = 0.5\kappa_{\text{SP}}$, and $\kappa = 0.2\kappa_{\text{SP}}$, respectively.

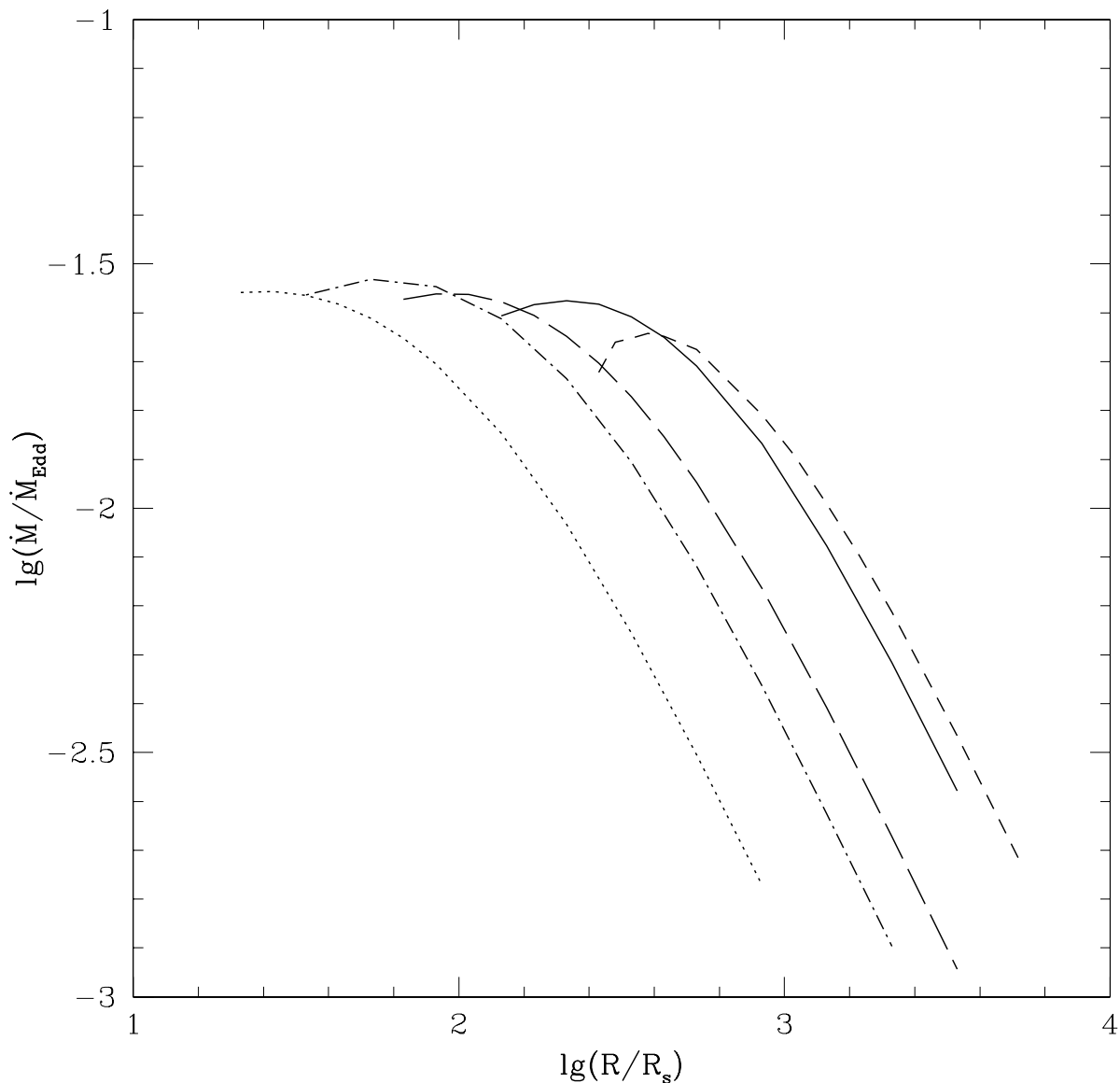


Fig. 6.— The composite influence of β and κ in the 2-T model, The solid line, long-dashed line, dash-dotted line and dotted line represent the cases of $(1/\beta = 0, \kappa = \kappa_{\text{Sp}})$, $(1/\beta = 0, \kappa = 0.5\kappa_{\text{Sp}})$, $(1/\beta = 0.3, \kappa = \kappa_{\text{Sp}})$, and $(1/\beta = 0.3, \kappa = 0.5\kappa_{\text{Sp}})$, respectively. The short-dashed line represents the result for $1/\beta = 0$ and $\kappa = \kappa_{\text{Sp}}$ in the 1-T model, which is plotted here for comparison.

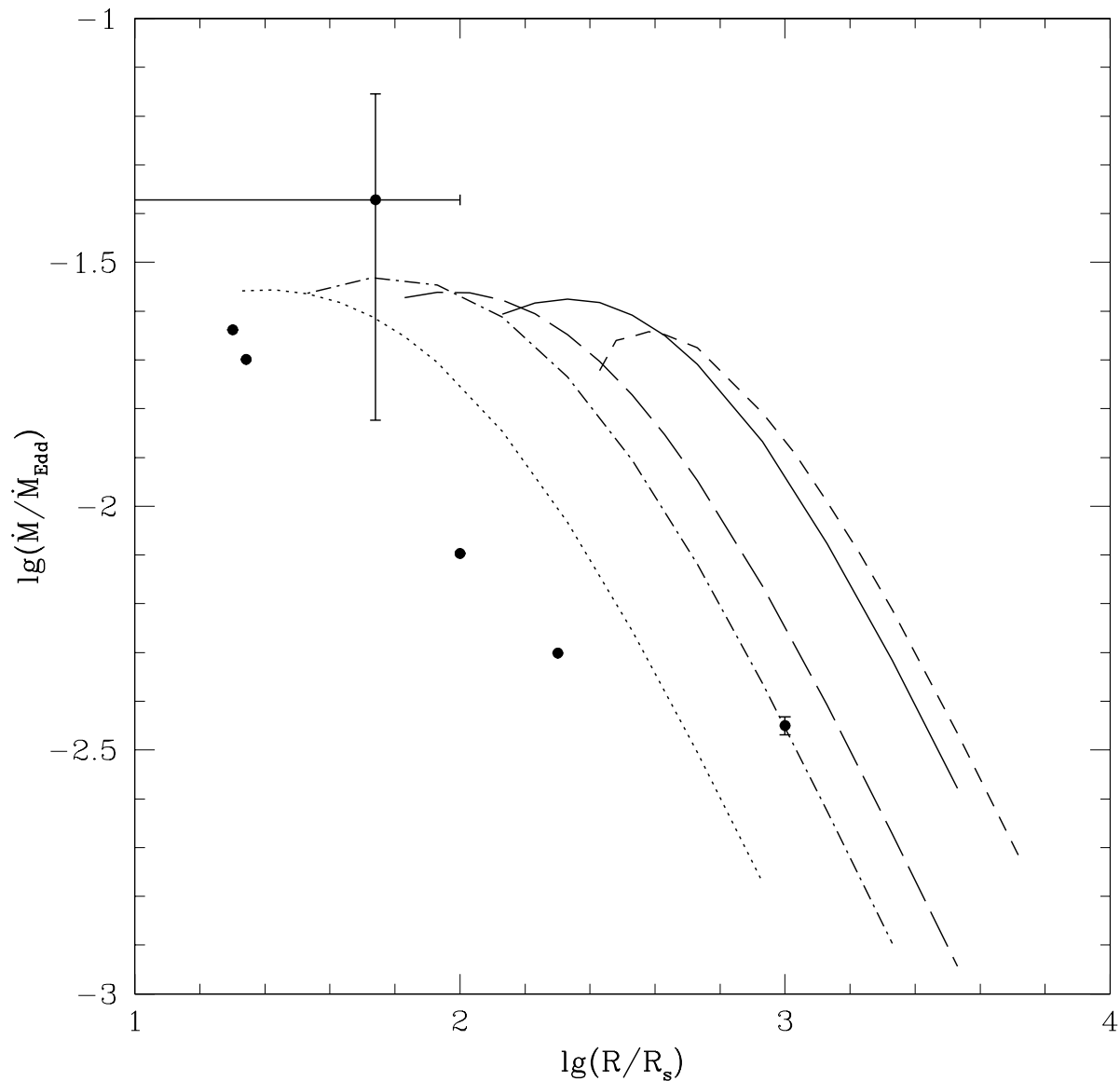


Fig. 7.— A comparison of the theoretical results and observations, The solid line represents the case of $1/\beta = 0$ and $\kappa = \kappa_{\text{Sp}}$. The long-dashed line represents the case of $\kappa = 0.5\kappa_{\text{Sp}}$ and $1/\beta = 0$. The dot-dashed line corresponds to the case of $1/\beta = 0.3$ and $\kappa = \kappa_{\text{Sp}}$. The dotted line is for $1/\beta = 0.3$ and $\kappa = 0.5\kappa_{\text{Sp}}$. The filled dots represent the data listed in Table 3.